Since January 2020 Elsevier has created a COVID-19 resource centre with free information in English and Mandarin on the novel coronavirus COVID-19. The COVID-19 resource centre is hosted on Elsevier Connect, the company's public news and information website.

Biochemical and Biophysical Research Communications 620 (2022) 180–187

Contents lists available at ScienceDirect

Biochemical and Biophysical Research Communications

journal homepage: www.elsevier.com/locate/ybbrc

Diabetic Covid-19 severity: Impaired glucose tolerance and pathologic bone loss

Jyotirmaya Behera [a], Jessica Ison [a], Michael J. Voor [b], Suresh C. Tyagi [a], Neetu Tyagi [a, *]

[a] Bone Biology Laboratory, Department of Physiology, School of Medicine, University of Louisville, Louisville, KY, 40202, USA
[b] Departments of Orthopaedic Surgery, University of Louisville, Louisville, KY, 40202, USA

ARTICLE INFO

Article history:
Received 28 May 2022
Accepted 14 June 2022
Available online 21 June 2022

Keywords:
SARS-CoV-2-RBD
Bone mineralization
miRNA regulation
Glucose intolerance
Insulin resistance
Diabetic bone loss

ABSTRACT

Diabetes mellitus (DM), hypertension, and cardiovascular diseases (CVDs) are the leading chronic comorbidities that enhance the severity and mortality of COVID-19 cases. However, SARS-CoV-2 mediated deregulation of diabetes pathophysiology and comorbidity that links the skeletal bone loss remain unclear. We used both streptozocin-induced type 2 diabetes (T2DM) mouse and hACE2 transgenic mouse to enable SARS-CoV-2-receptor binding domain (RBD) mediated abnormal glucose metabolism and bone loss phenotype in mice. The data demonstrate that SARS-CoV-2-RBD treatment in pre-existing diabetes conditions in hACE2 (T2DM + RBD) mice results in the aggravated osteoblast inflammation and downregulation of Glucose transporter 4 (Glut4) expression via upregulation of miR-294−3p expression. The data also found increased fasting blood glucose and reduced insulin sensitivity in the T2DM + RBD condition compared to the T2DM condition. Femoral trabecular bone mass loss and bone mechanical quality were further reduced in T2DM + RBD mice. Mechanistically, silencing of miR-294 function improved Glut4 expression, glucose metabolism, and bone formation in T2DM + RBD + anti-miR-294 mice. These data uncover the previously undefined role of SARS-CoV-2-RBD treatment mediated complex pathological symptoms of diabetic COVID-19 mice with abnormal bone metabolism via a miRNA-294/Glut4 axis. Therefore, this work would provide a better understanding of the interplay between diabetes and SARS-CoV-2 infection.

1. Introduction

A novel severe acute respiratory syndrome coronavirus 2 (SARS-CoV-2) was first detected in the Wuhan city of China at the end of 2019 [1]. SARS-CoV-2 is found to cause coronavirus disease 2019 (COVID-19) in human. The world health organization (WHO) classified COVID-19 as a worldwide pandemic on March 11, 2020 (2). Following COVID-19 infection, the severity of the disease ranges from asymptomatic to pneumonia and is followed by acute respiratory distress syndrome [2]. A retrospective cohort study suggested that age is one of the critical risk factors for comorbidity and mortality due to SARS-CoV-2. Additionally, chronic diseases like cardiovascular disease (CVD), kidney disease, obesity, and diabetes are associated with hospital admission and unfavorable outcomes during COVID-19 infection [1]. The study has suggested that type 2 diabetes mellitus (T2DM) and cardiovascular disease are the leading two comorbidities that worsen COVID-19 pathology [3]. In addition, this study suggested that CVDs and T2DM are associated with 22.7% and 19.7% mortality rates in COVID-19 patients, respectively. Therefore, it is essential to understand the reciprocal influences between comorbidities and COVID-19 to control and treat these diseases.

Despite much has been addressed in the pulmonary system during COVID-19, less is known about COVID-19 infection on extra-pulmonary systems in diabetic comorbidity, particularly its effects on the skeletal system. There are several putative mechanisms that drive the SARS-CoV-2 and cause a negative function on the skeletal system. SARS-CoV-2 utilizes as its entry receptor, human angiotensin-converting enzyme 2 (hACE2) is expressed in bone cells [4]. Hypocalcemia, a condition with a reduced plasma level of calcium, is common among COVID-19 patients and is predicted to have a disease severity [5]. Therefore, these studies prompted us to explore the fundamental mechanism of diabetic comorbidity on bone microstructural damage and aggravation of abnormal glucose

* Corresponding author. FAPS Bone Biology Laboratory, Department of Physiology, Health Sciences Center, A-1201, University of Louisville Louisville, KY, 40202, USA.
E-mail address: n0tyag01@louisville.edu (N. Tyagi).

https://doi.org/10.1016/j.bbrc.2022.06.043
0006-291X/

metabolism in a hACE2-transgenic (Tg) mouse model of COVID-19 infection.

In the present study, we used B6.Cg-Tg(K18-ACE2)2Prlmn/J mice (K18-hACE2 Tg mice for generating COVID-19 pathophysiology under T2DM condition. Since most of the SARS-CoV-2 variants are unable to effectively cause severity in mice, therefore, we have obtained humanized mice model that expresses human ACE2 (hACE2) in airway cells. In the current study, we generated a co-morbid mice model of T2DM with SARS-CoV-2 severity and investigated the consequences of the RBD effect on the skeletal system of K18-hACE2 mice. The study found that SARS-Cov-2 RBD treatment resulted in abnormal glucose tolerance, insulin resistance, and significantly increased trabecular bone loss and bone mechanical quality in T2DM mice. Mechanistically, increased calprotectin (S100a8/9) expression in osteoblast was associated with reduced glucose transporter 4 (Glut4 or SLC2A4) expression through upregulation of miRNA-294−3p expression. Silencing miRNA-294 function through specific anti-miR-294 or siRNA against S100a9 prevents the SARS-Cov-2 RBD induced down-regulation of Glut4 expression. Further, the data investigated that anti-miR-294 potently improves glucose metabolism and rescues the loss of the trabecular bone mass and bone mechanical quality in diabetic comorbidity (K18-hACE2- T2DM + RBD) mice.

2. Methods

2.1. Animals

Eight-week-old female C57BL/6J and B6.Cg-Tg(K18-ACE2) 2Prlmn/J mice (K18-hACE2 Tg mice were purchased from the Jackson Laboratory (Bar Harbor, ME). All animals were maintained on a 12-h light and 12-h dark cycle in the animal facility of the University of Louisville. Mice were given free access to water and standard ingredient chow (solid). The study protocol of the diabetes induction and other experimental procedures was approved by the Institutional Animal Care and Use Committees (IACUC) of the University of Louisville.

3. Diabetes induction

At eight weeks of age, the K18-hACE2 Tg mice were fed either a nonfat control diet (called NFD or control WT) or a high-fat diet (HFD, 42%; D12492; Research Diets Inc., USA) for 8 weeks. The HFD contained 42% fat (corn oil and lard), 28% protein, and <1% carbohydrate. To induce T2DM in the HFD group [6], mice have been treated every alternative day with streptozotocin (STZ, Sigma) (50 mg/kg/body weight) through intraperitoneal (i.p.) injections or saline injections (total of 6 injections) for 2-weeks. At the end of the treatment regimen, body weight, and fasting blood glucose levels were performed. To study the impacts of SARS-CoV2-RBD treatment on T2DM disease, SARS-CoV-2-RBD (SAE1000, Sigma) was administrated to the hACE2 Tg-T2DM mice at the concentration of 0.1 μg/ml via an intranasal route (total 2 injections) for a week and post-treatment induced complex pathological symptoms of diabetic severity and abnormal bone catabolism was being observed.

The following group of mice was employed for experimental studies.

- K18-hACE2 mice (as WT)
- K18-hACE2 fed with a high-fat diet + STZ (Type 2 diabetes or T2DM)
- SARS-CoV-2-RBD treated T2DM mice (T2DM + RBD)
- Anti-miR-294 supplemented T2DM + RBD mice (T2DM + RBD + anti-miR-294)

3.1. Primary osteoblast culture and differentiation

Following the removal of bone marrow (BM) cells, the whole femoral bones were cut into small pieces and digested under collagenase solution (1 mg/ml). The isolated primary osteoblasts were cultured under an alpha minimum essential medium (α-MEM; Invitrogen) supplemented with 15% heat-inactivated FBS, 100 U/mL penicillin/streptomycin. After 72 h of culture, non-adherent cells were washed using 1X PBS. The adherent cells were further maintained until got confluence.

3.1.1. Alkaline phosphatase assay and calcium nodule assay

ALP activity and in vitro mineralization staining were performed according to our previously published protocol [7]. Briefly, passaged primary osteoblasts were cultured under an osteogenic induction medium (OIM; α-MEM+15% FBS supplemented with 2 mM β-glycerophosphate, 100 nM dexamethasone, and 50 μg/mL ascorbic acid), for 21 days. On 7 days of osteogenic induction, cells were fixed with 70% ethanol and stained with ALP (Sigma). Similarly, for calcium nodule formation, 21 days of cultured osteoblasts were fixed with 70% ethanol and stained with 1.5% ARS. Then cells were photographed on a phase-contrast microscope.

3.2. Gene expression using qPCR

Gene expression analysis was performed as previously described [8,9]. Total RNA was isolated from whole bone tissues using TRIzol Reagent (15-596-018, Invitrogen™). The cDNA was synthesized using total RNA (1 μg) following the instruction of the ImProm-II™ Reverse Transcription System manufacturer's protocol (A3800, Promega). Primers (forward and reverse) against target genes of interest were used for real-time PCR detection and are listed in Table 1.

3.3. microRNA profiling by RT2 miRNA PCR array

Total RNA was isolated from femoral bone tissue using the miRNeasy Mini Kit (Qiagen, USA). Total RNA (1 μg/ml) was converted to cDNA using the miScript II RT kit (Qiagen). The RT2-qPCR array of the experimental samples was performed on 96-well plates (MIMM-005Z, miScript miRNA PCR Array Mouse diabetes, Qiagen), according to the manufacturer's instructions. Target individual microRNA expression is amplified from cDNA samples using a miScript SYBR Green PCR kit in Stratagene Mx3000p (Agilent Technologies). The obtained Ct values were expressed in fold change in expression.

Table 1
Sequences of PCR primers used for real-time quantitative PCR.

Gene	Primer Sequences (5′→3′)
Mouse G6Pase	FP: GATGTCCTGGAGGATGAAGTGG RP: GTGGTGGTGTTCACCTCCTGAA
Mouse PEPCK	FP: TTTAGGGCGCATTCCTCATC RP: TGTCCTTGTGGATTGAAAGGAC
Mouse Glut4	FP: GCGCTCTGTCTCTCTGACCT RP: ACCTTATTGCCCTCCTGCTT
Mouse S100a8	FP: GAGACAGACATCCGGAGGAGA RP: GTGGGATGTGAACACGGAAGA
Mouse S100a9	FP: GGATGAAATCTCTCGCGTTT RP: GGTTATGGGCAGAGATTGCTT
Mouse miR-294−3p	FP: ACTGAGGAGGCCACCCAAGGA RP: TGAAGAGGACCAGAACGATGAG
Mouse GAPDH	FP: TGCACCACCAACTGCTTGC RP: GGCATGGACTGTAGTCAGAG

3.4. In silico analysis

To predict potential targets of miR-294–3p at the mouse SLC2A4/Glut4 mRNA region, in silico analyses were performed using Targetscan (http://www.targetscan.org/). The predicted consequential pairing of the target gen region at 3′-UTR (top) and miRNA (bottom) was obtained.

3.5. AntagomiR-294 injection and overexpression of SLC2A4/Glut4

To investigate the role of miR-294–3p on Glut4 function in diabetic comorbidity mice, the miRNA inhibitors or synthetic antagomiRs against the miR-294–3p (cat 4464084; Thermo Scientific) or the negative control (cat 4464076; Thermo Scientific) were purchased and delivered via intravenous (i.v) tail-vein injections (2 μg per injection) 3-times per week (total 6 injections). Moreover, to overexpress Glut4 expression, osteoblasts were transfected with Glut4/SLC2A4 cDNA ORF Clone (100 ng; SinoBiological) using a Lipofectamine 3000 reagent (Invitrogen). Glut4 overexpression in osteoblasts culture was confirmed with qPCR analysis.

3.6. MicroCT analysis of bone

The femur bones were excised and collected for the micro-CT analysis as our previously described protocol [10]. The femurs of the mice were scanned using micro-CT (μCT 40, Scanco Medical, Switzerland). The femoral micro-architectural parameters such as bone mineral density (BMD, mg/cm3), bone volume/trabecular volume (BV/TV), trabecular number (Tb.N), trabecular thickness (Tb.Th), and trabecular separation (Tb.Sp) were analyzed using Inveon Research Workplace III software.

3.7. Statistical analysis

All statistical analyses and graphical presentations were performed with GraphPad Prism software, v.9.0.0. All experimental data are expressed as the mean ± S.E.M. The significant differences in more than two experimental groups were compared by one-way analysis of variance (ANOVA) in combination with Tukey's multiple comparison test. $P < 0.05$ was considered statistically significant. Experiments were repeated three times independently.

4. Results

4.1. SARS-CoV-2 RBD treatment suppresses glucose transporter 4 (Glut4) expression via calprotectin dependent inflammation in diabetic mice

Ten-week-old female hACE2-diabetic mice administrated SARS-CoV-2 RBD (0.1 μg/ml) or vehicle control by the intranasal route and allowed to keep under observation for 2 weeks (Fig. 1a). A previous study suggested that calprotectin is a serum marker of inflammation and found to be elevated in various conditions such as inflammation, infection, and cancer [11]. However, the interplay between calprotectin and SARS-CoV-2 infection was not known. Therefore, we performed calprotectin ELISA to study its level in the T2DM + SARS-CoV-2 RBD condition. The data demonstrated that calprotectin level was significantly increased in both serum and primary osteoblast of the T2DM and T2DM + SARS-CoV-2 RBD (T2DM + RBD) condition compared to the WT condition (Fig. 1b and c). Besides, serum levels of IL-6 and TNF-α cytokines were significantly increased in T2DM + RBD conditions compared to T2DM (Supplementary Figs. S1a and b), indicating a strong response of inflammation is induced in T2DM + RBD conditions. We then tested the mRNA expressions of S100a8 and S100a9, which codes calprotectin protein, and found that the above mRNA expressions increased significantly in the T2DM + RBD condition compared to the T2DM condition alone (Fig. 1d).

We performed a qPCR-based miRNA array to further discover the potent miRNAs which are differentially expressed in isolated osteoblasts in the T2DM + RBD condition. The data found that several miRNAs were indeed differentially regulated in the experimental condition, as depicted in hierarchical clustering analysis (Fig. 1e). Interestingly, miR-294–3p were simultaneously upregulated in the T2DM + RBD and T2DM conditions compared to the WT control condition (Fig. 2e, black arrowhead). Using qPCR analysis, we further validated that the expression of miR-294–3p was significantly upregulated ($p < 0.0001$) in the T2DM + RBD condition (Fig. 1f). To functionally link the miR-294–3p expression with the calprotectin level, we silenced the S100a9 expression using the siRNA-mediated knockdown approach (siS100a9 or si-a9) in T2DM + RBD mice. The data showed that si-a9 treatment inhibited the expression of miR-294–3p in the T2DM + RBD condition compared to the T2DM + RBD condition (Fig. 1f). To understand whether miR-294–3p could regulate Glut4 (SLC2A4) expression in femoral bone tissue, an in silico TargetScan analysis was performed. The study found that the miR-294–3p sequence recognized the 59–65 bp of the conserved sequence of the 3′-UTR regions of the Glut4 (Fig. 1g). In addition, qPCR data confirmed that targeted inhibition of the miR-294–3p expression by AntagomiR-294–3p or si-a9 treatment significantly increased the Glut4 expression in the T2DM + RBD + anti-miR-294–3p or T2DM + RBD + si-a9 conditions compared to the T2DM alone (Fig. 1h). These data suggested calprotectin facilitated down-regulation of Glut4 expression through upregulation of miR-294–3p in the skeleton of T2DM + RBD comorbid mice.

Preexisting Diabetes Exacerbates Glucose Intolerance and Insulin Resistance in SARS-CoV-2 RBD Treated Mice.

The intranasal route of administrating SARS-CoV-2 RBD in the T2DM mouse had no effect on the body weight compared to T2DM mice, whereas T2DM + RBD + anti-miR-294–3p mice significantly decreased the body weight compared to the T2DM + RBD alone (Fig. 2a). T2DM + RBD mice also had reduced glucose metabolism (GTT; glucose tolerance test) and insulin tolerance (ITT; glucose tolerance test) compared to T2DM mice alone. However, silencing the miR-294–3p expression, improved the glucose metabolism and insulin tolerance in T2DM + RBD + anti-miR-294–3p mice compared to T2DM + RBD mice (Fig. 2b and c). In line with these findings, T2DM + RBD + anti-miR-294–3p mice showed reduced levels of plasma glycemia (both fasting glucose and glucose fed condition) and plasma insulin after fasting compared to T2DM + RBD mice (Fig. 2d–e, f). As expected, HbA1c (%) levels were significantly reduced in T2DM + RBD + anti-miR-294–3p mice compared to T2DM + RBD mice (Fig. 2g).

We further analyzed the mRNA expression of gluconeogenesis enzymes (G6Pase and Pepck) in the liver extracts and found that G6Pase and Pepck expression was reduced in the T2DM + RBD + anti-miR-294–3p mice (Fig. 2h). Furthermore, we tested glucose uptake capacity in osteoblast culture in vitro. Briefly, osteoblasts from T2DM + RBD mice were transfected with Glut4/SLC2A4 cDNA ORF Clone. After 24 h of post-transfection, cells were administrated with 2-NBDG, a fluorescence probe for 12 h. The data showed that the glucose uptake capacity of osteoblasts was significantly improved in the T2DM + RBD + Glut4 and T2DM + RBD + anti-miR-294–3p conditions compared to the T2DM + RBD condition (Fig. 2i). These data suggested that preexisting diabetes with SARS-CoV-2 RBD treatment devastates the diabetic pathophysiology by regulating poor glucose metabolism and insulin tolerance via the miR-294-3p-Glut4 axis.

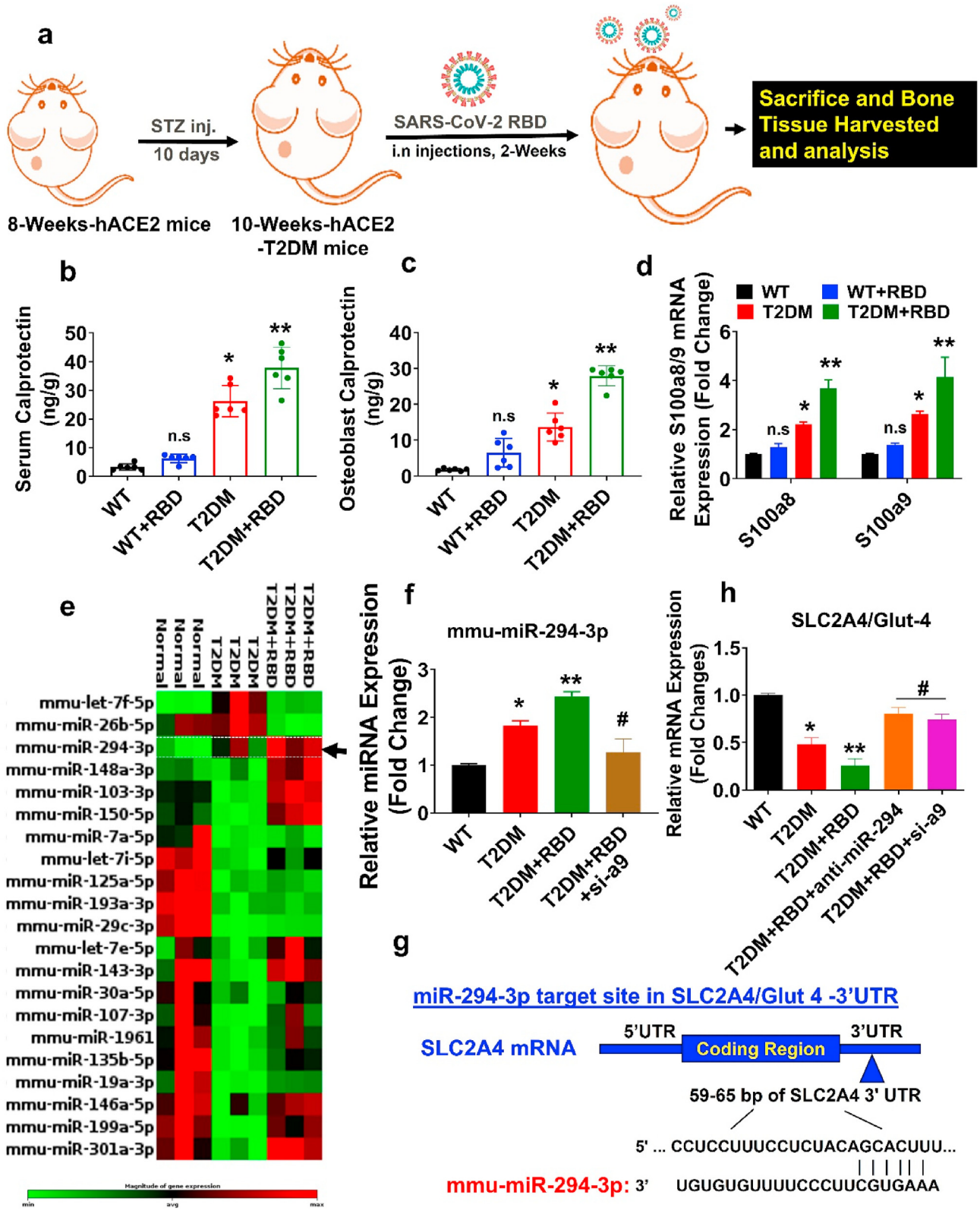

Fig. 1. SARS-CoV-2 RBD treatment suppresses the Glut4 expression in osteoblast via calprotectin-dependent inflammation in diabetic mice. (a) Ten-week-old female hACE2-T2DM mice were administrated SARS-CoV-2 RBD recombinant protein or vehicle control by the intranasal route and tissue was harvested after 2 weeks. (b–c) ELISA assay of calprotectin level in serum and osteoblast lysate. (d) S100a8/a9 gene expression by qPCR. (e) Heat map of differentially expressed miRNAs in osteoblast by qPCR Array. (f) qPCR validation of miR-294–3p. (g) Targetscan analysis of the miR-294–3p binding sites in 3′-UTR of the SLC2A4/Glut4. (h) qPCR analysis of Glut4 expression. Experiments were repeated at least three times. Data are expressed as mean ± SEM. n = 6 mice per group. *p < 0.05 compared with the WT control, **p < 0.05 compared with the T2DM, $^{\#}p \leq 0.05$ compared with the T2DM + RBD.

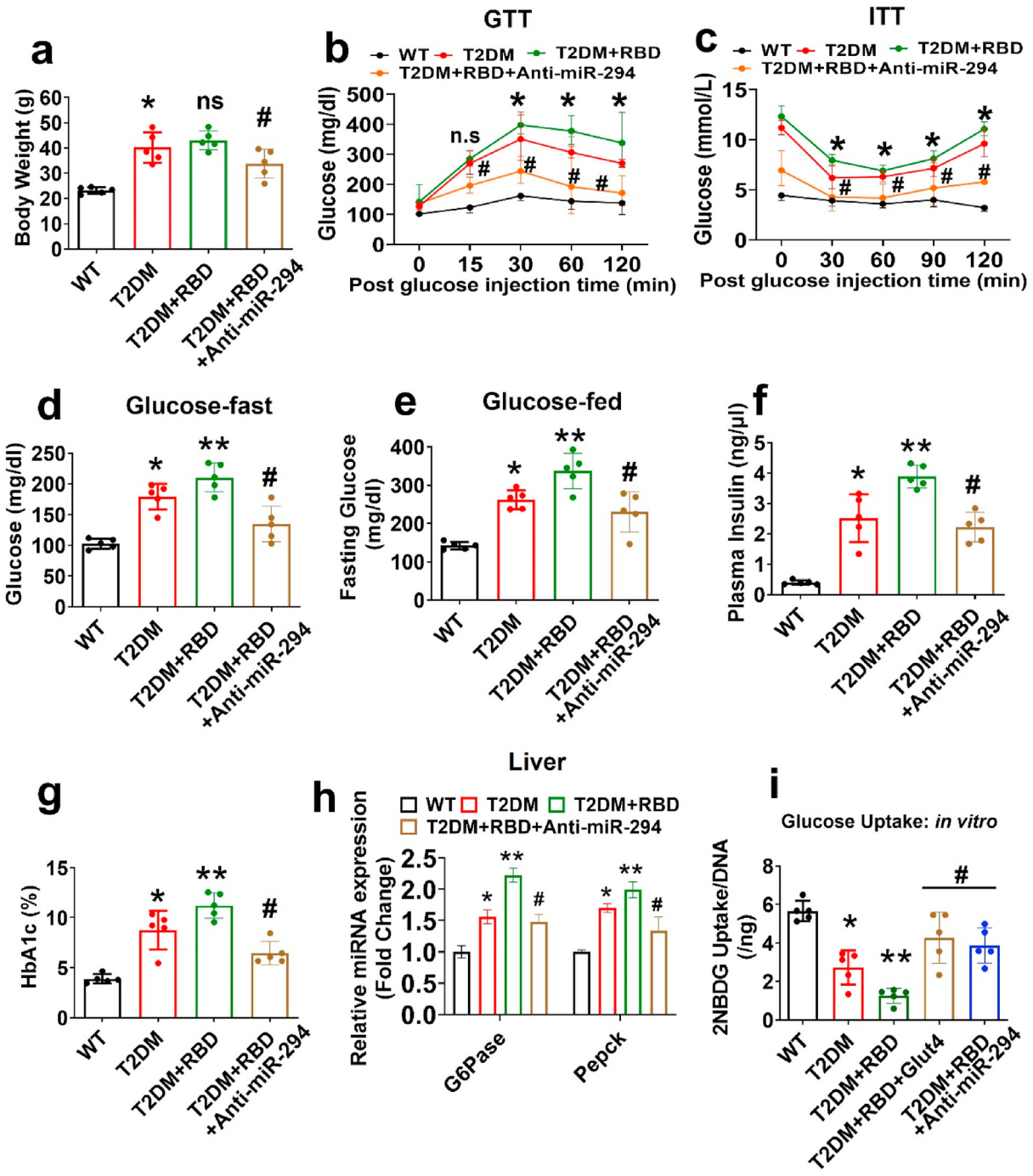

Fig. 2. Preexisting diabetes worsens insulin resistance and glucose intolerance in SARS-CoV-2 RBD treated mice. (a) Bodyweight (BW) was measured. (b–c) Glucose tolerance test (GTT) and insulin tolerance test (ITT) in the experimental mice. (d–e) Fasting glucose and glucose-fed conditions were monitored. (f–g) Plasma insulin and blood HbA1c (%) level was measured. (h) qPCR analysis of G6Pase and Pepck in liver tissue. (i) 2-NBDG uptake assay in osteoblast. Experiments were repeated at least three times. Data are expressed as mean ± SEM. n = 5 mice per group. *p < 0.05 compared with the WT control, **p < 0.05 compared with the T2DM, #p ≤ 0.05 compared with the T2DM + RBD.

4.2. SARS-CoV-2 RBD treatment suppresses osteogenesis in vitro

To evaluate the potentially devastating effect of SARS-CoV-2 RBD in osteoblast mineralization, primary osteoblast was cultured under OIM for 21 days. The data demonstrate that the cell proliferation capacity was indeed suppressed in both T2DM and T2DM + RBD conditions compared to the WT condition. However, the above changes were improved in the T2DM + RBD + anti-miR-294–3p condition (Fig. 3a). On day 6 and day 21 of osteogenic induction, cultured primary osteoblast exhibited an increase in ALP activity and mineralized nodule formation in the T2DM + RBD + anti-miR-294–3p condition compared to the T2DM + RBD condition (Upper and Lower panel, Fig. 3b–d). Further, the mRNA transcripts expression of osteogenic genes (Osx, and Bglap) were significantly improved in the osteoblast of the T2DM + RBD + anti-miR-294–3p condition on Day 21 (Fig. 3e). Besides, overexpression of Glut4 in cultured osteoblast significantly improves the ALP, bone mineralization capacity, and expression of

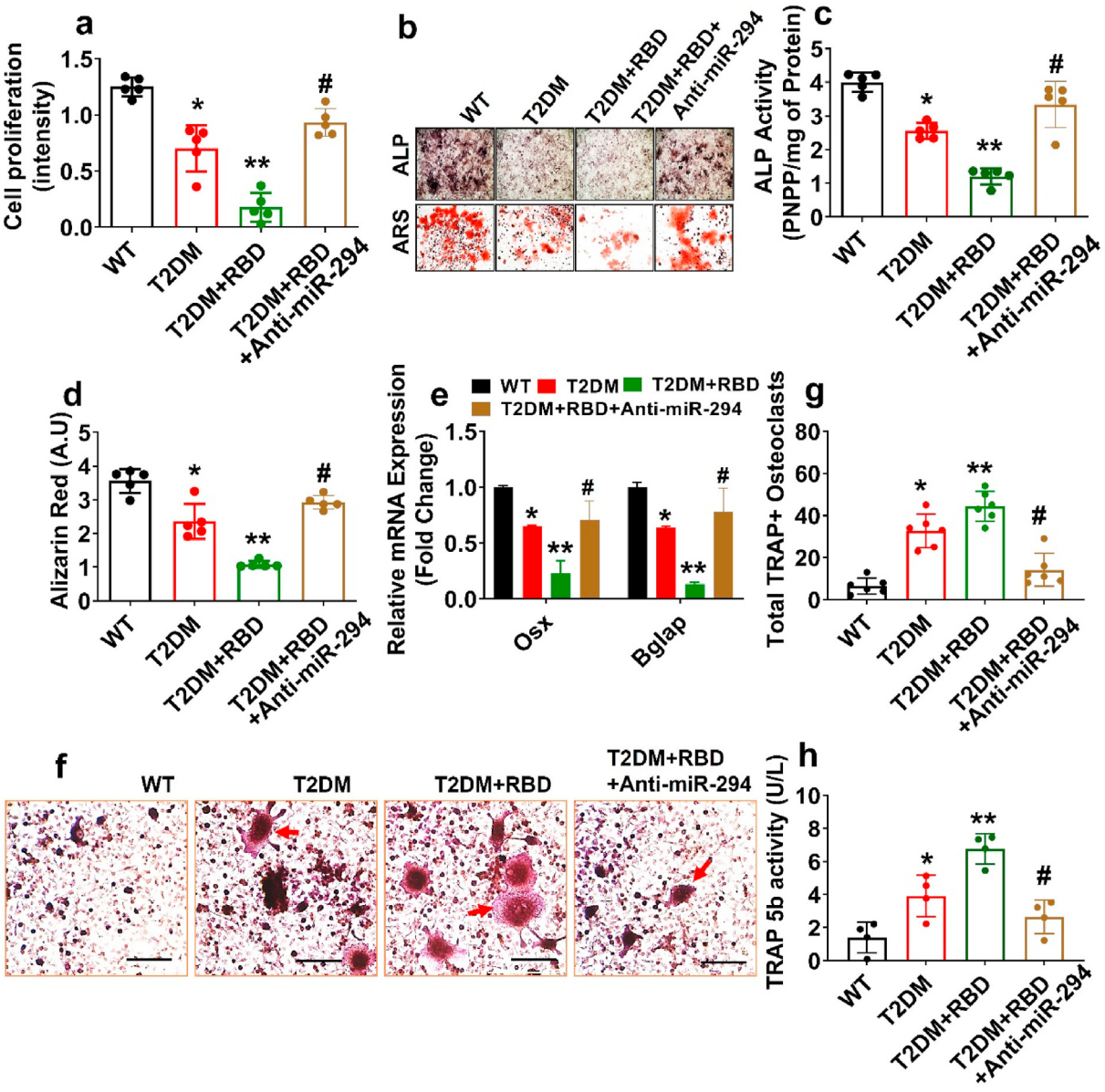

Fig. 3. SARS-CoV-2 RBD treatment dampens osteogenesis in T2DM mice. (a) Cell proliferation by MTT assay. (b–d) ALP and ARS assay on day 6 and day 21. Scale bar: 200 μm. (c–d) The bar graph represents the ALP activity and calcium nodule assay by ARS. (e) qPCR analysis of Osx and Bglap mRNA expression. (f–g) TRAP + stained osteoclasts culture. Scale bar: 200 μm. The red arrow indicates matured TRAP + osteoclasts. The bar graph represents the total number of TRAP + osteoclasts (g). (h) TRAP-5b activity in the osteoclast lysates. Experiments were repeated at least three times. Data are expressed as mean ± SEM. n = 5 mice per group. *p < 0.05 compared with the WT control, **p < 0.05 compared with the T2DM, #p ≤ 0.05 compared with the T2DM + RBD. (For interpretation of the references to colour in this figure legend, the reader is referred to the Web version of this article.)

the osteogenic genes (Osx and Bglap) in the T2DM + RBD + Glut4 condition (Supplementary Figs. S2a–c). Thus, SARS-CoV-2 RBD administration substantially diminished the osteoblast differentiation and mineralization in the T2DM mice via the miR-294/Glut4 axis (Fig. 3a–e).

Furthermore, we demonstrated ex vivo osteoclastogenesis assays by using a conditioned medium (CM) from day 7 osteoblast culture. The data showed that T2DM + RBD-CM treated osteoclast cultures had more mature, tartrate-resistant acid phosphatase–positive (TRAP+) osteoclasts (red arrow) by Day 4 of differentiation, when compared to T2DM-CM. However, the above changes were mitigated in the T2DM + RBD + anti-miR-294-3p-CM (Fig. 3f and g). TRAP 5b activity was also significantly reduced in the osteoclast of the T2DM + RBD + anti-miR-294-3p-CM condition compared to the T2DM + RBD-CM condition (Fig. 3h). These studies conclude that the T2DM + RBD condition exaggerated osteoclastogenesis through paracrine signaling.

4.3. SARS-CoV-2 RBD treatment worsened bone loss and mechanical quality in diabetes comorbid mice

To determine whether administration of anti-miR-294 in the promotion of bone homeostasis, T2DM + RBD mice were administrated with anti-miR-294 via intravenous (i.v) tail-vein injections or vehicle control to T2DM + RBD mice for 2 weeks (Fig. 4a). At the end of the treatment, femoral bones were analyzed by microCT scans (Fig. 4b). The data showed that distal femur BMD, BV/TV ratio, Tb.N, and Tb.Th was reduced in the T2DM + RBD mice compared to T2DM mice (Fig. 4b–e). However, Tb.Sp was found to be significantly increased in T2DM + RBD mice compared to the T2DM mice

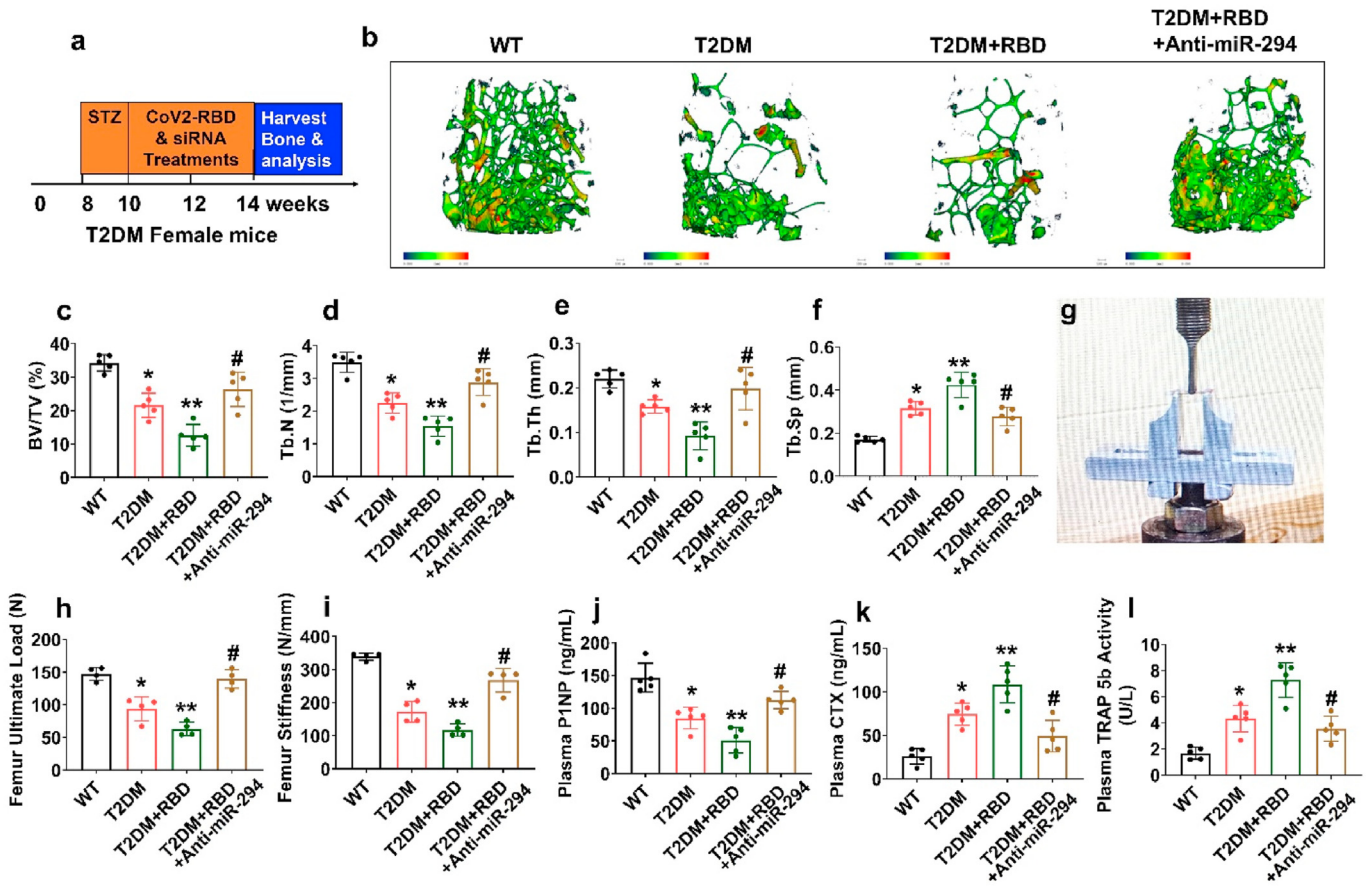

Fig. 4. SARS-CoV-2 RBD treatment exacerbates pathologic bone loss in T2DM mice. (a) Anti-miR-294 was IV injected into T2DM + RBD mice. The femoral bone samples were harvested, and downstream analyses were performed. (b) MicroCT scan analysis of the distal femur of the experimental mice. Scale bar, 100 μm. (c–f) Trabecular bone phenotype parameters were observed: BMD, BV/TV (%), Tb.N (1/mm), Tb.Th (mm), Tb.Sp (mm). (g–i) Bone mechanical properties such as (Maximum load (N) and stiffness (N/mm)) were analyzed. (j–l) ELISA analysis of P1NP, CTX-I, and TRAP-5b activity was tested. Experiments were repeated at least three times. Data are expressed as mean ± SEM. n = 5 mice per group. *p < 0.05 compared with the WT control, **p < 0.05 compared with the T2DM, #p ≤ 0.05 compared with the T2DM + RBD.

(Fig. 4b, f), indicating a strong osteoporotic phenotype was observed. However, silencing the miR-294 function in those T2DM + RBD mice prevented the comorbidity-associated bone loss in the T2DM + RBD + anti-miR-294–3p mice (Fig. 4b–f). Interestingly, bone mechanical properties, such as maximum load and stiffness, were improved in the T2DM + RBD + anti-miR-294–3p mice compared to T2DM + RBD mice as assessed by the 3-point bending test (Fig. 4g–i).

Furthermore, bone formation marker, P1NP, and bone resorption marker CTX were decreased and increased in the plasma of the T2DM + RBD mice respectively. Besides, plasma TRAP-5b activity was significantly reduced in T2DM + RBD mice. However, the above effect was mitigated in the T2DM + RBD + anti-miR-294–3p mice (Fig. 4j-l). These data demonstrate that silencing miR-294 function in the osteoblast of the T2DM + RBD mice improves bone formation and bone mechanical quality.

6. Discussion

In the current study, we provided evidence first time that K18-hACE2 Tg mice with diabetes (called T2DM) and T2DM + RBD mice are characterized by increased systemic levels of calprotectin. Mechanistically, T2DM + RBD mice regulate calprotectin-miR-294–3p axis mediated downregulation of Glut4 expression in the osteoblast. This leads to insulin resistance and glucose intolerance. On the other hand, overexpression of Glut4 expression and miR-294–3p inhibition significantly improves glucose metabolism and subsequently increases bone formation and mechanical quality in the T2DM + RBD mice. Our study identifies a previously undefined role of miR-294–3p as a downstream regulator of calprotectin signaling participating in the diabetes comorbidity associated with abnormal glucose metabolism and pathologic bone loss in T2DM mice during SARS-CoV-2 RBD Treatment.

A recent study has suggested that patients with preexisting chronic diseases like CVD and T2DM were found to be at increased risk of COVID-19 infection [12]. Others have suggested that both CVD and T2DM are the hallmark of comorbidity that accentuate the COVID-19 severity and mortality [3,13,14]. Therefore, it is necessary to understand the complex pathological symptoms of COVID-19 patients with preexisting CVD and T2DM. Taking this into account, we generated a comorbid mouse (K18-hACE2 Tg-T2DM + RBD) model to mimic the clinical symptoms of T2DM patients infected with SARS-CoV-2 infection. Our T2DM comorbid mice exhibited severe inflammatory response via a calprotectin-dependent manner (Fig. 1). This observation may explain the pneumonia-like symptoms of comorbid patients. In this study, we further emphasized to study of the target organ, like bone, and the potential pathologic mechanisms in T2DM comorbid mice models.

A recent report suggested that among the 1099 COVID-19 patients in China, 26.9% of patients are T2DM and achieve severity and death compared to 6.1% of patients with no primary disease. This study clearly suggests that hyperglycemia is linked with adverse outcomes of SARS-CoV-2 infections. Other have suggested that SARS-CoV-2 infection further exhibit the blood glucose level in the

patients [15]. However, the specific mechanism of SARS-CoV-2 infection on the regulation of glucose intolerance and insulin resistance and subsequently bone loss remains unknown. Here, we observed altered fasting blood glucose, GTT, and ITT responses in T2DM + RBD mice through deregulation of the miR-294/Glut4 axis. Besides, serum calprotectin (Fig. 1) and cytokines (IL-6, TNF-α) were higher in the T2DM + RBD mice (Supplementary S1), which was often referred to as a cytokine storm.

We and others have previously reported that abnormal glucose metabolism is associated with skeletal loss in obese mice [16–18]. However, the bridge between abnormal glucose production and skeletal loss through SARS-CoV-2 infection is not studied yet. In the current study, we found that T2DM + RBD comorbid mice showed reduced osteoblast mineralization, loss of trabecular bone mass, and bone mechanical properties by promoting osteoclastogenesis (Figs. 3 and 4). Intriguingly, inhibition of both calprotectin and miR-294–3p function in T2DM + RBD mice prevents abnormal glucose metabolism and restoration of bone mass. These results suggest that T2DM patients with SARS-CoV-2 infection are likely at a high risk of poor outcomes with osteoporosis phenotype and need more intensive care at the hospital.

In summary, we characterized the exaggerated effect of SARS-CoV-2 RBD on abnormal glucose metabolism and bone homeostasis using the hACE2 Tg-T2DM mouse model. Our co-morbid mouse model showed a bone-specific and systemic inflammatory response that result in glucose intolerance, and insulin resistance and subsequently causes bone loss via regulating the calprotectin-miRNA-294–3p/Glut4 axis. Our study provides clues to understanding the development of a promising therapeutic strategy against T2DM + RBD-associated bone loss.

Declaration of interests

The authors declare the following financial interests/personal relationships which may be considered as potential competing interests: Neetu Tyagi reports financial support was provided by National Institutes of Health.

Acknowledgment

This research study was supported, in part, by the National Institute of Health (NIH) grant AR-067667 to NT.

Appendix A. Supplementary data

Supplementary data to this article can be found online at https://doi.org/10.1016/j.bbrc.2022.06.043.

References

[1] D.A. Sirin, F. Ozcelik, The relationship between COVID-19 and the dental damage stage determined by radiological examination, Oral Radiol. 37 (4) (2021 Oct) 600–609.
[2] Y. Ma, D. Lu, L. Bao, Y. Qu, et al., SARS-CoV-2 infection aggravates chronic comorbidities of cardiovascular diseases and diabetes in mice, Animal Model Exp. Med. 4 (1) (2021 Mar 6) 2–15.
[3] Epidemiology Working Group for NCIP Epidemic Response, Chinese Center for Disease Control and Prevention, The epidemiological characteristics of an outbreak of 2019 novel coronavirus diseases (COVID-19) in China, Zhonghua Liuxingbingxue Zazhi 41 (2) (2020 Feb 10) 145–151.
[4] N. Zamorano Cuervo, N. Grandvaux, ACE2: evidence of role as entry receptor for SARS-CoV-2 and implications in comorbidities, Elife 9 (2020 Nov 9), e61390.
[5] L. Di Filippo, A.M. Formenti, P. Rovere-Querini, M. Carlucci, et al., Hypocalcemia is highly prevalent and predicts hospitalization in patients with COVID-19, Endocrine 68 (3) (2020 Jun) 475–478.
[6] H. Karasawa, S. Nagata-Goto, K. Takaishi, Y. Kumagae, A novel model of type 2 diabetes mellitus based on obesity induced by high-fat diet in BDF1 mice, Metabolism 58 (3) (2009 Mar) 296–303.
[7] J. Behera, J. Ison, H. Rai, N. Tyagi, Allyl sulfide promotes osteoblast differentiation and bone density via reducing mitochondrial DNA release mediated Kdm6b/H3K27me3 epigenetic mechanism, Biochem. Biophys. Res. Commun. 543 (2021 Mar 5) 87–94.
[8] J. Behera, S.C. Tyagi, N. Tyagi, Hyperhomocysteinemia induced endothelial progenitor cells dysfunction through hyper-methylation of CBS promoter, Biochem. Biophys. Res. Commun. 510 (1) (2019 Feb 26) 135–141.
[9] J. Behera, K.E. Kelly, M.J. Voor, N. Metreveli, et al., Hydrogen sulfide promotes bone homeostasis by balancing inflammatory cytokine signaling in CBS-deficient mice through an epigenetic mechanism, Sci. Rep. 8 (1) (2018 Oct 15), 15226.
[10] J. Behera, J. Ison, M.J. Voor, N. Tyagi, Probiotics stimulate bone formation in obese mice via histone methylations, Theranostics 11 (17) (2021 Jul 25) 8605–8623.
[11] M. Jarlborg, D.S. Courvoisier, C. Lamacchia, L. Martinez Prat, et al., Physicians of the Swiss Clinical Quality Management (SCQM) registry. Serum calprotectin: a promising biomarker in rheumatoid arthritis and axial spondyloarthritis, Arthritis Res. Ther. 22 (1) (2020 May 6) 105.
[12] T.J. Guzik, S.A. Mohiddin, A. Dimarco, V. Patel, et al., COVID-19 and the cardiovascular system: implications for risk assessment, diagnosis, and treatment options, Cardiovasc. Res. 116 (10) (2020 Aug 1) 1666–1687.
[13] S. Ruan, Likelihood of survival of coronavirus disease 2019, Lancet Infect. Dis. 20 (6) (2020 Jun) 630–631. Erratum in: Lancet Infect Dis. 2020 Apr 6.
[14] The Novel Coronavirus Pneumonia Emergency Response Epidemiology Team, The epidemiological characteristics of an outbreak of 2019 novel coronavirus diseases (COVID-19) - China, 2020, China CDC Wkly 2 (8) (2020 Feb 21) 113–122.
[15] C.H. Mazucanti, J.M. Egan, SARS-CoV-2 disease severity and diabetes: why the connection and what is to be done? Immun. Ageing 17 (2020 Jun 30) 21.
[16] J. Behera, J. Ison, M.J. Voor, N. Tyagi, Probiotics stimulate bone formation in obese mice via histone methylations, Theranostics 11 (17) (2021 Jul 25) 8605–8623.
[17] L. Shu, E. Beier, T. Sheu, H. Zhang, et al., High-fat diet causes bone loss in young mice by promoting osteoclastogenesis through alteration of the bone marrow environment, Calcif. Tissue Int. 96 (4) (2015 Apr) 313–323.
[18] S. Kim, H. Henneicke, L.L. Cavanagh, E. Macfarlane, et al., Osteoblastic glucocorticoid signaling exacerbates high-fat-diet- induced bone loss and obesity, Bone Res. 9 (1) (2021 Sep 1) 40.